Optomechanics of random media

S. Gentilini[1,*] and C. Conti[1,2]
[1]*Institute for Complex Systems, National Research Council (ISC-CNR), Via dei Taurini 19, 00185 Rome, Italy*
[2]*Dipartimento di Fisica - Università La Sapienza, P. A. Moro 2, 00185, Roma, Italy*
(Received 10 December 2014; published 9 April 2015)

Using light to control the movement of nanostructured objects is a great challenge. This challenge involves fields like optical tweezing, Casimir forces, integrated optics, biophysics, and many others. However, when the complexity of the light-activated devices increases, disorder unavoidably occurs and induces a number of effects, such as multiple-scattering, diffusion, and the localization of light. We show that these effects radically enhance the mechanical effect of light. We determine theoretically the link between optical pressure and the light diffusion coefficient and unveil that optical forces and their statistical fluctuations reach a maximum at the onset of the photon localization. Disorder may thus be exploited for increasing the mechanical action of light on complex objects.

DOI: 10.1103/PhysRevA.91.043813 PACS number(s): 42.50.Wk, 42.25.Dd, 42.25.Fx

Several recent investigations show that light propagation and amplification in disordered matter can be controlled. This possibility allows applications such as tunable random lasers, transmission through random media, and novel disorder-driven devices, such as paper-based lasers and ultrasensitive spectrometers [1–7]. Controlling the photon-transport also enables us to tailor the optical properties of new materials [8,9], although effects like the three-dimensional (3D) Anderson localization of light are still largely debated [10–12]. However, there is a specific field in which the benefits of randomness have not yet been investigated, and that is optomechanics. Even if the concept of optical pressure dates back to the famous work of Kepler on comet tails in the 16th century [13], the role of light diffusion and localization on the optomechanical forces (OMFs) in disordered matter is unexplored.

Following James Clerk Maxwell [14], many theoretical and experimental efforts were devoted in the past to OMFs [15–21], with applications in laser cooling [22,23], optical manipulation [24–27], biophysics [28,29], and optomechanical devices [30,31]. OMFs are due to the interaction of the electromagnetic (EM) field with the boundaries of dielectric objects. Random systems are characterized by a large number of boundaries, and determining OMFs can be highly nontrivial. However, in the perspective of optically activated nanostructured devices, understanding OMFs due to many interfaces and to the related multiple scattering of light is pivotal.

In the absence of scattering, any photon that is transmitted unaltered through a dielectric material does not furnish kinetic momentum to matter [32,33]. If the scattering changes the photon direction, a recoil force appears. In the presence of multiple scattering, the photon random walk generates a random walk of the medium. This problem is remarkably similar to the random walk of a macroscopic object in a liquid [34]: even if the timescale of the single molecule collision is very fast, the statistical fluctuations of the number of collisions generate a slow observable motion of the macroscopic object. For the photon, we find that the temporal fluctuations of the forces occur on a timescale much longer than the optical carrier period, and that the physics is made even richer by localization effects. Indeed, when the photon-transport mean-free path ℓ_{tr} is small enough, 3D disordered systems can support long-living localized states [35–39]. The excitation of these states reduces the transmission $\mathcal{T}$ and, in turn, affects the radiation pressure p (i.e., the longitudinal component of the force) according to the well-known equation

$$p = \frac{1-\mathcal{T}}{2c_0} I_0, \tag{1}$$

with c_0 being the vacuum light speed and I_0 being the input optical intensity [20,33].

In this work, we show that disorder-induced localized states increase the OMFs. By using the Maxwell stress tensor method (MSTM), we find the relationship between the OMFs exerted on the entire disordered system and the parameters characterizing the photon-transport regime: the dynamic diffusion constant and the Thouless conductance [40], as obtained by considering the propagation in the random medium of an ultrashort pulse. Because of the small values of the OMFs, one must consider dielectric systems with spatial dimensions of the order of tens of wavelengths. Larger systems are not substantially affected by OMFs. In small disordered systems, EM localized states are strongly altered by finite-size effects. The most rigourous way to deal with finite-size effects is a fully vectorial solution of Maxwell equations. The diffusion approximation, which allows us to describe light propagation in large random systems, cannot be adopted. In the following, we describe our numerical results obtained by a parallel computational approach for solving the Maxwell equations. Our numerical approach is based on a finite-difference-time-domain (FDTD) algorithm [41] with typical runs involving thousands of processors in an IBM Blue Gene/Q system with a massively parallel architecture. Other authors have previously calculated by FDTD techniques the optical pressure on dielectric media [42–46].

We consider a cubic structure with dimensions $L_x = L_y = L_z = L$, made by a random distribution of 100 nm radius monodispersed dielectric spheres with refractive index n. We consider three different sizes of the cubic box, $L = 0.5$, 1.0, and 2.0 μm; and we vary the refractive index of the single particle in an interval ranging from $n = 1.5$ to 3.5. We solve the

*silvia.gentilini@roma1.infn.it

time-dependent Maxwell's equation in 3D spatial dimensions:

$$\nabla \times \mathbf{E} = -\mu_0 \partial_t \mathbf{H}, \quad \nabla \times \mathbf{H} = \partial_t \mathbf{D}, \tag{2}$$

where $\mathbf{D}$ is the displacement vector given by $\mathbf{D} = \epsilon_0 \epsilon_r \mathbf{E}$, and $\epsilon_r = n^2$. We make two series of simulations by launching two different x-polarized excitation signals on the 3D structure: (i) we use a continuous wave (cw) light beam with wavelength $\lambda = 600$ nm to calculate the OMFs by the MSTM; (ii) we use a light pulse of duration $t_0 = 10$ fs, with a spectral content centered at $\lambda = 600$ nm to characterize the photon-transport regime. Both the signals are launched along the z direction and impinge on the input facet of the assembly located at $z = 0$. The output facet is placed at $z = L$.

Let Σ and V be the surface area and the volume of the block, respectively. The time-dependent force due the EM wave, neglecting electrostriction, is given by [47]

$$\mathbf{F} = \frac{d\mathbf{G}_{\text{mech}}}{dt} = \int_\Sigma \overline{\overline{\mathbf{S}}} \cdot \hat{\mathbf{n}} dA - \frac{1}{c^2} \frac{d}{dt} \int_V \mathbf{E} \times \mathbf{H} dV, \tag{3}$$

where $\overline{\overline{\mathbf{S}}} \cdot \hat{\mathbf{n}} = \epsilon \mathbf{E}(\mathbf{E} \cdot \hat{\mathbf{n}}) + \mu \mathbf{H}(\mathbf{H} \cdot \hat{\mathbf{n}}) - \frac{1}{2}(\epsilon E^2 + \mu H^2)\hat{\mathbf{n}}$ is the projection of the Maxwell stress tensor $\overline{\overline{\mathbf{S}}}$ on the unitary normal $\hat{\mathbf{n}}$ exiting from the surface Σ. The last term in Eq. (3) is the time-derivative of the EM momentum in the volume V, whose density is $\mathbf{g}$ and given by the Abraham and von Laue expression $\mathbf{g} = \mathbf{g}_A = \frac{1}{c^2}\mathbf{E} \times \mathbf{H}$ [48]. In the cw case the time-average force is given by $\overline{\mathbf{F}} = \frac{1}{T}\int_{-T/2}^{T/2} \mathbf{F} dt$, with the optical cycle $T = \lambda/c$. $\overline{\mathbf{F}}$ gives the amount of momentum per unit time transferred to the block. In the pulsed case, the time-average is defined as $\overline{\mathbf{F}} = \frac{1}{T}\int_{-\infty}^{\infty} \mathbf{F} dt$, which gives the total momentum transferred to the block per pulse during a normalization time T much longer than the pulse duration.

We calculate the following output quantities: (i) the three components of the resulting electromagnetic force $\overline{\mathbf{F}}$ acting on the whole random assembly of dielectric beads; (ii) the transverse [in the (x,y) plane] intensity distribution of the electric field at the output, at $z = L$, plane; and (iii) the total transmission $T(t)$ calculated by integrating the z component of the Poynting vector over the output (x,y) plane. Notice that the first two quantities are obtained by the cw simulations, while the latter is obtained by using pulsed excitation.

Figure 1(a) shows the sketch of the simulated system. The random assembly of dielectric spheres is illuminated by a 1 μm waist cw laser beam; light scattered by the random structures in all directions is also indicated. The image in Fig. 1(b) displays the typical intensity spatial distribution of the electric field at the output (x-y) plane ($z = L$). Figure 1(c) shows the time dynamics of the force $F_z(t)$ for $L = 2$ μm and $n = 1.5$. The fast oscillations correspond to the optical carrier of the exciting source; the superimposed curve (thick line) is obtained by filtering out such oscillations. The time-dynamics of the filtered signal looks as a square-wave pulse due to the initial transient, which is needed by the EM wave to propagate through the whole structure. After this initial transient a stationary regime takes place. Notice that the stationary value of the longitudinal force is different from zero.

When the index contrast between the beads and the surrounding medium (vacuum) increases, the recoil force edge in the pulse is smoothed. Figure 1(d) shows the effect of the

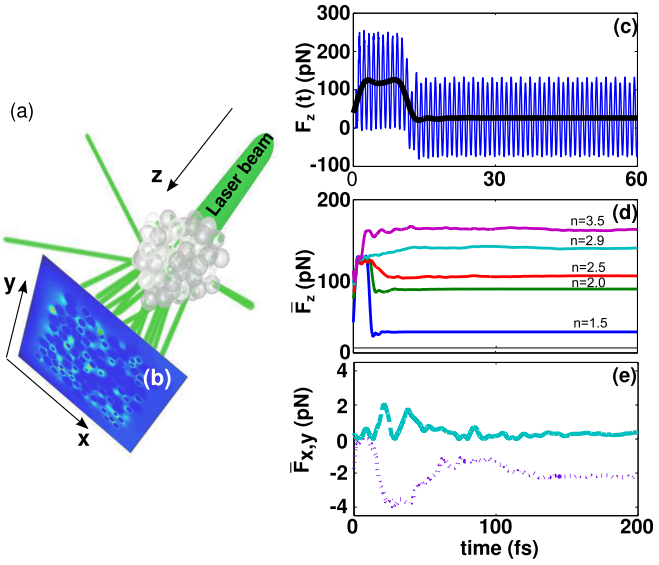

FIG. 1. (Color online) (a) Sketch of the physical system considered in the 3D-FDTD numerical simulations. (b) Intensity spatial distribution of the output electric field. (c) Time-dynamics of the OMF z component $F_z(t)$: the fast oscillations are due to the optical carrier period of the light source; the superimposed thick curve is obtained by spectral filtering the fast oscillations. (d) Time-dynamics of disorder averaged $\overline{F}_z(t)$ for different particle refractive indices n and fixed system length $L = 2.0$ μm. (e) As in panel (d) for the transverse components $\overline{F}_x(t)$ (dotted line) and $\overline{F}_y(t)$ (continuous line) for $n = 2.5$ particle refractive index.

scattering on the time behavior of $\overline{F}_z(t)$ for a specific disorder realization. As anticipated, when n grows, the trajectory of the photons follows a complex path, which affects $\overline{F}_z(t)$.

Figure 1(e) shows the temporal behavior of the filtered transverse components $\overline{F}_{x,y}(t)$ for a given particle refractive index $n = 2.5$ and system size $L = 2$ μm. Because of the random walk due to the multiple scattering, the photons escaping from the lateral sides of the sample generate transverse OMFs components. When averaging over several disorder realizations, these components vanish; this transverse random force is expected to be observable for a specific sample with a fixed disorder realization. In order to determine the statistical distribution of the OMFs, we repeated the CW simulations for sixty different disorder realizations for any considered system size L and refractive index n.

The lateral leakages of photons increase with the scattering strength; this reduces the recoil force in the z direction and increases the overall longitudinal force. Such a dynamics is confirmed by the behavior of the disorder average optical force z component, $\langle \overline{F}_z(t) \rangle$, reported in Figs. 2(a)–2(c) for different L and n. Figure 2(d) shows the stationary value of the $\langle \overline{F}_z(t) \rangle$ curves reported in Figs. 2(a)–2(c) versus n. This stationary value is normalized with respect to the correspondent homogeneous structure (i.e., a cubic block of the same size of the random assembly and refractive index). Notice that, for the largest sample ($L = 2.0$ μm), one can identify a refractive index threshold at which the longitudinal force in the disordered case is enhanced with respect to the homogeneous case.

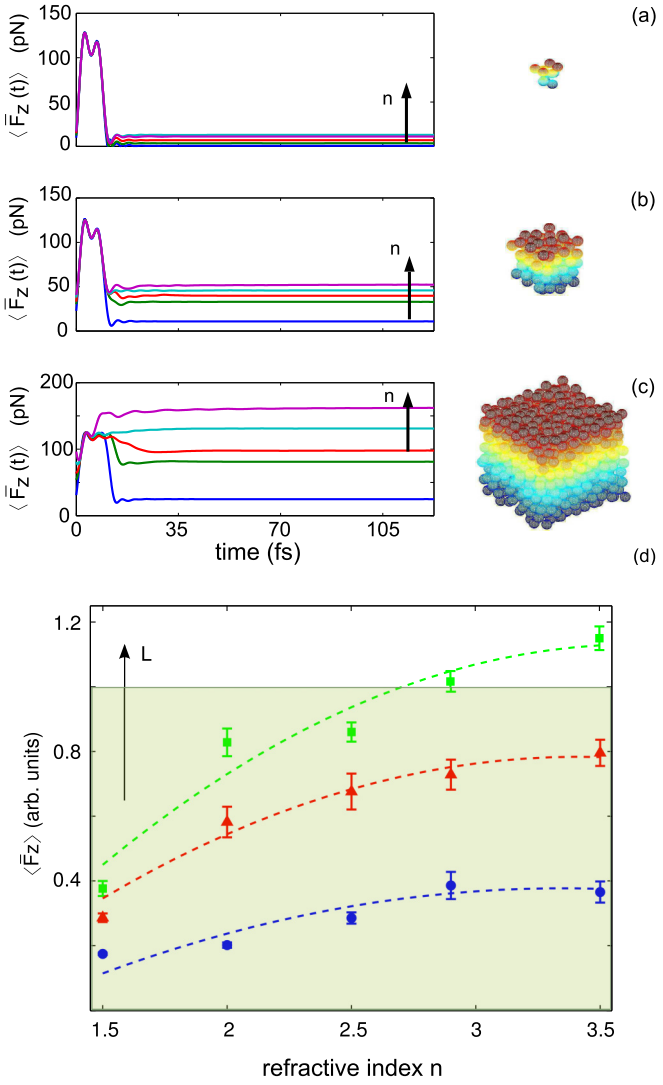

FIG. 2. (Color online) Disorder-averaged $\langle \overline{F}_z(t) \rangle$ for the different system sizes (a) $L = 0.5$ μm, (b) 1.5 μm, and (c) 2.0 μm. Each curve corresponds to a different particle refractive index $n = 1.5$, 2.0, 2.5, 2.9, and 3.5 (from bottom to top). The 3D structures in the panels are representatives of the simulated assemblies. (d) Stationary long-time value of the curves reported in panels (a)–(c), $\langle \overline{F}_z \rangle$, normalized with respect to the corresponding homogeneous case vs the refractive index n. Each curve refers to a different size of the system: $L = 0.5$ μm (•), 1.0 μm (▲), and 2.0 μm (■). The colored box marks the transition at which the OMF z component is enhanced by the disorder.

We then analyze the transverse components, $\overline{F}_x(t)$ and $\overline{F}_y(t)$. Figures 3(a)–3(d) show the statistical distributions of the stationary values of $\overline{F}_x$ and $\overline{F}_y$. Notice that the histograms broaden with the increase of the refractive index and that this effect is more evident for the largest sizes. This analysis predicts that a specific disorder realization sustains a transverse force at a random direction. This result may be related to the known enhancement of the fluctuations of the transmission at the photon localization [49].

In order to link the OMFs with the photon dynamics, i.e., with the transition towards a localized regime expected at large

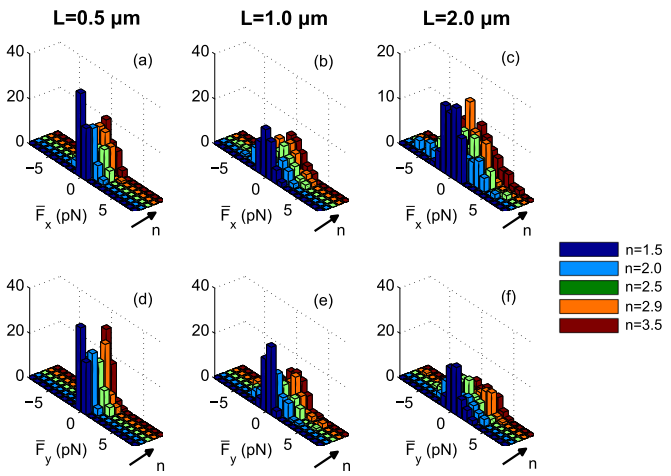

FIG. 3. (Color online) Histograms of the stationary long-time value of the transverse (x,y) components of the optomechanical force, $\overline{F}_x$ and $\overline{F}_y$ as obtained for 60 different disorders. Each panel corresponds to a given size of the system, (a), (d) $L = 0.5$ μm, (b), (e) 1.0 μm, and (c), (f) 2.0 μm.

n, we perform a set of simulations by considering an input EM pulse with duration $t_0 = 10$ fs and central wavelength $\lambda = 600$ nm. Following the procedure in Ref. [36], we determine the photon-transport mean-free path as $\ell_{tr} = 3D/v_E$ [50], where v_E is the energy propagation velocity given by $v_E = L/\Delta t$ with L being the sample length and Δt being the time spent by the pulse peak to travel from the input ($z = 0$) to the output ($z = L$) face of the sample. By analyzing the trailing edge of the total transmission $T(t)$, collected at the output facet of the system, we calculate the diffusion coefficient as $D = L^2/(\pi^2\tau)$, with τ being the exponential decay time of $T(t)$. Figure 4(a) shows the photon-transport mean-free path ℓ_{tr} versus n for the $L = 1.0$ μm (circles) and $L = 2.0$ μm (dashed line) samples; Fig. 4(b) reports the product $k\ell_{tr}$, between the wave vector $k = 2\pi/\lambda$ of the incident radiation and the photon-transport mean-free path ℓ_{tr} of Fig. 4(a). Figure 4(c) shows the diffusion constant D versus n for the sample length $L = 1.0$ μm (circles) and $L = 2.0$ μm (triangles). Figure 4(d) shows the disorder average OMFs z component versus D. An enhancement of the OMFs is found when the diffusion constant reduces. The OMFs reach a maximum when D reaches the smallest value in correspondence of the localization transition. This result clearly shows the relation between the OMFs and the photons dynamics within a disordered 3D medium. Notice that, in order to calculate the forces, one needs to consider a spatially limited structure for which the diffusion constant does not vanish because of the finite-size effects.

In order to further characterize the photon-transport regime, following the scaling theory of localization in 3D systems [40], we analyze the spectral content of the output electric field when varying the system size. Figures 4(c)–4(e) report the output EM spectra corresponding to samples with $n = 3.5$ and $L = 0.5$, 1.0, and 2.0 μm. When increasing L, the spectra display an increasing number of peaks. The linewidth of these resonances narrows with L, signaling the formation of long-living localized modes. A measure of the localization degree

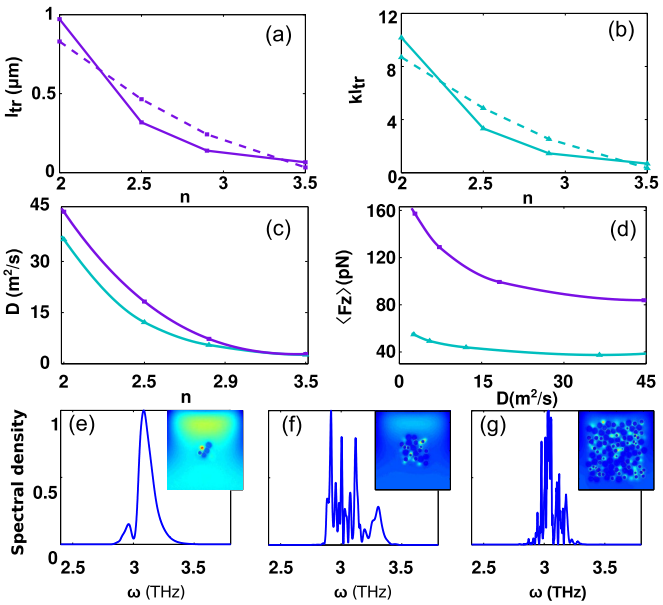

FIG. 4. (Color online) (a) Photon-transport mean-free path ℓ_{tr} versus n for the system sizes $L = 1.0\ \mu$m (continuous line) and $2\ \mu$m (dashed line). (b) Product $k\ell_{tr}$ versus n obtained from the panel (a) for the system size $L = 1\ \mu$m (continuous line) and $L = 2\ \mu$m (dashed line). (c) Diffusion coefficient D vs n obtained for the system sizes $L = 1.0\,\mu$m (■) and $L = 2.0\,\mu$m (▲). (d) Stationary value of the $\langle \overline{F}_z \rangle$ vs diffusion coefficient D for $L = 1.0\ \mu$m (▲) and $L = 2.0\ \mu$m (■) system sizes. (e)–(g) Spectral content of the output electric field for the highest particle refractive index ($n = 3.5$) and different system sizes (e) $L = 0.5\ \mu$m, (f) $L = 1.0\ \mu$m, and (g) $L = 2.0\ \mu$m. The dimensionless conductance g is also indicated. The insets show the intensity spatial distributions of the output electric fields in the (x,y) plane at $z = L$.

is given by the Thouless conductance

$$g(L) = \frac{\delta\omega}{\Delta\omega},$$

where $\delta\omega$ is the peak spectral width and $\Delta\omega$ is the peak distance. The Thouless conductance is calculated by averaging over all the modes. The localization transition occurs when $g < 1$ [40], a condition that is found when $n = 3.5$ and $L = 1.0$ and $2.0\ \mu$m. For these values, the output intensity profile of the electric field in the (x,y) plane is reported in Figs. 4(e)–4(g). We remark that $g > 1$ for all the considered cases with $n < 3.5$. This result shows that, for $g < 1$, the force reaches a maximum. This maximum can be explained by recalling that the longitudinal force per unit transverse area (optical pressure) increases when the total transmission of the sample decreases [33]. The abatement of transmission is specifically expected at the onset of photon localization [40].

In conclusion, to unveil the effect of disorder on the optomechanical forces, we have used a massively parallel computational approach. This approach was combined with the analysis of the light-transport regime of ultrashort pulses by the Thouless conductance, the dynamic diffusion coefficient, and the photon-transport mean-free path. When increasing the strength of disorder, we observe the broadening of the statistical distribution of the force transverse components. Correspondingly, the diffusion constant and the photon-transport mean-free path decrease and the optical pressure reaches a maximum. This maximum shows that the momentum transferred to a disordered micron-sized composite object increases when approaching a localized regime. The optomechanical action is enhanced at the onset of the photon localization of light. These findings open the road to the exploitation of light scattering and localization for controlling the motion of complex dielectric structures. A proper arrangement of refractive index distribution, loss, shape, size, and spatial configuration of dielectric particles, allows us to tailor the photon Brownian motion. One can thus engineer the random walk of photons to determine the light-induced forces for several applications as micromotors and photonics robots.

We acknowledge support from the CINECA under the ISCRA initiative, from the Progetto di Ateneo Sapienza Award: PhotoAnderson and from the European Research Council, project VANGUARD, grant agreement 664782.

[1] M. Leonetti, C. Conti, and C. Lopez, Nat. Photonics **5**, 615 (2011).
[2] I. M. Vellekop and A. P. Mosk, Opt. Lett. **32**, 2309 (2007).
[3] J. Bertolotti, E. G. van Putten, C. Blum, A. Lagendijck, W. L. Vos, and A. Mosk, Nature (London) **491**, 232 (2012).
[4] N. Bachelard, J. Andreasen, S. Gigan, and P. Sebbah, Phys. Rev. Lett. **109**, 033903 (2012).
[5] V. Folli, N. Ghofraniha, A. Puglisi, L. Leuzzi, and C. Conti, Sci. Rep. **3**, 2251 (2013).
[6] N. Ghofraniha, I. Viola, F. Di Maria, G. Barbarella, G. Gigli, and C. Conti, Laser Photonics Rev. **7**, 432 (2013).
[7] B. Redding, S. F. Liew, R. Sarma, and H. Cao, Nat. Photonics **7**, 746 (2013).
[8] P. D. Garcia, R. Sapienza, A. Blanco, and C. Lopez, Adv. Mater. **19**, 2597 (2007).
[9] H. Noh, J.-K. Yang, S. F. Liew, M. J. Rooks, G. S. Solomon, and H. Cao, Phys. Rev. Lett. **106**, 183901 (2011).
[10] S. John, Phys. Rev. Lett. **58**, 2486 (1987).
[11] D. S. Wiersma, P. Bartolini, A. Lagendijk, and R. Righini, Nature (London) **390**, 671 (1997).
[12] S. E. Skipetrov and I. M. Sokolov, Phys. Rev. Lett. **112**, 023905 (2014).
[13] J. Kepler, *De cometis libelli tres. Augsburg: Andrea Apergeri* (1619), https://archive.org/stream/den-kbd-pil-130011021221-001#page/n16/mode/2up.
[14] J. C. Maxwell, *A Treatise on Electricity and Magnetism* (Clarendon Press, New York, 1904).
[15] P. N. Lebedev, Ann. Phys. (Berlin, Ger.) **6**, 433 (1901).
[16] E. F. Nichols and G. F. Hull, Phys. Rev. **17**, 26 (1903).
[17] H. Minkowski, Nachr. Ges. Wiss. Göttn Math.-Phys. Kl. **53**, 472 (1908).

[18] M. Abraham, Rendiconti del Circolo Matematico di Palermo **28**, 1 (1909).
[19] A. Einstein, Phys. Z. **18**, 121 (1917).
[20] P. W. Milloni and R. W. Boyd, Adv. Opt. Photonics **2**, 519 (2010).
[21] H. B. Chan, V. A. Aksyuk, R. N. Kleiman, D. J. Bishop, and F. Capasso, Science **291**, 1941 (2001).
[22] O. Arcizet, P.-F. Cohadon, T. Briant, M. Pinard, and A. Heidmann, Nature (London) **444**, 71 (2006).
[23] S. Gigan, H. R. Böhm, M. Paternostro, F. Blaser, G. Langer, J. B. Hertzberg, K. C. Schwab, D. Bäuerle, M. Aspelmeyer, and A. Zeilinger, Nature (London) **444**, 67 (2006).
[24] D. B. Phillips, M. J. Padgett, S. Hanna, Y.-L. D. Ho, D. M. Carberry, M. J. Miles, and S. H. Simpson, Nat. Photonics **8**, 400 (2014).
[25] A. Ashkin, Phys. Rev. Lett. **40**, 729 (1978).
[26] K. Dholakia and P. Zemnek, Rev. Mod. Phys. **82**, 1767 (2010).
[27] R. W. Bowman, G. M. Gibson, M. J. Padgett, F. Saglimbeni, and R. Di Leonardo, Phys. Rev. Lett. **110**, 095902 (2013).
[28] S. Unterkofler, M. K. Garbos, T. G. Euser, and P. S. J. Russell, J. Biophotonics **6**, 743 (2013).
[29] N. Koumakis, A. Lepore, C. Maggi, and R. Di Leonardo, Nat. Commun. **4**, 2588 (2013).
[30] M. K. Garbos, T. G. Euser, O. A. Schmidt, S. Unterkofler, and P. S. J. Russell, Opt. Lett. **36**, 2020 (2011).
[31] A. Butsch, C. Conti, F. Biancalana, and P. S. J. Russell, Phys. Rev. Lett. **108**, 093903 (2012).
[32] N. L. Balazs, Phys. Rev. **91**, 408 (1953).
[33] C. Conti and R. Boyd, Phys. Rev. A **89**, 033834 (2014).
[34] A. Einstein, Ann. Phys. (Berlin, Ger.) **17**, 549 (1905).
[35] M. Storzer, P. Gross, C. M. Aegerter, and G. Maret, Phys. Rev. Lett. **96**, 063904 (2006).
[36] S. Gentilini, A. Fratalocchi, L. Angelani, G. Ruocco, and C. Conti, Opt. Lett. **34**, 130 (2009).
[37] S. Gentilini, A. Fratalocchi, and C. Conti, Phys. Rev. B **81**, 014209 (2010).
[38] J. Wang and A. Genack, Nature (London) **471**, 345 (2011).
[39] T. Sperling, W. Buhrer, C. Aegerter, and G. Maret, Nat. Photonics **7**, 48 (2013).
[40] P. Sheng, *Scattering and Localization of Classical Waves in Random Media* (World Scientific, Singapore, 1990).
[41] A. Taflove and S. C. Hagness, *Computational Electrodynamics: the Finite-Difference Time-Domain Method* (Artech House, Boston, 2000).
[42] W. Collett, C. Ventrice, and S. Mahajan, Appl. Phys. Lett. **82**, 2730 (2003).
[43] D. Zhang, X. Yuan, S. Tjin, and S. Krishnan, Opt. Express **12**, 2220 (2004).
[44] R. Gauthier, Opt. Express **13**, 3707 (2005).
[45] W. Sun, S. Pan, and Y. Jiang, J. Mod. Opt. **53**, 2691 (2006).
[46] S.-Y. Sung and Y.-G. Lee, Opt. Express **16**, 3463 (2008).
[47] I. Brevik, Phys. Rep. **52**, 133–201 (1979).
[48] S. M. Barnett, Phys. Rev. Lett. **104**, 070401 (2010).
[49] A. A. Chabanov, M. Stoytchev, and A. Z. Genack, Nature (London) **404**, 850 (2000).
[50] S. E. Skipetrov and B. A. van Tiggelen, Phys. Rev. Lett. **96**, 043902 (2006).